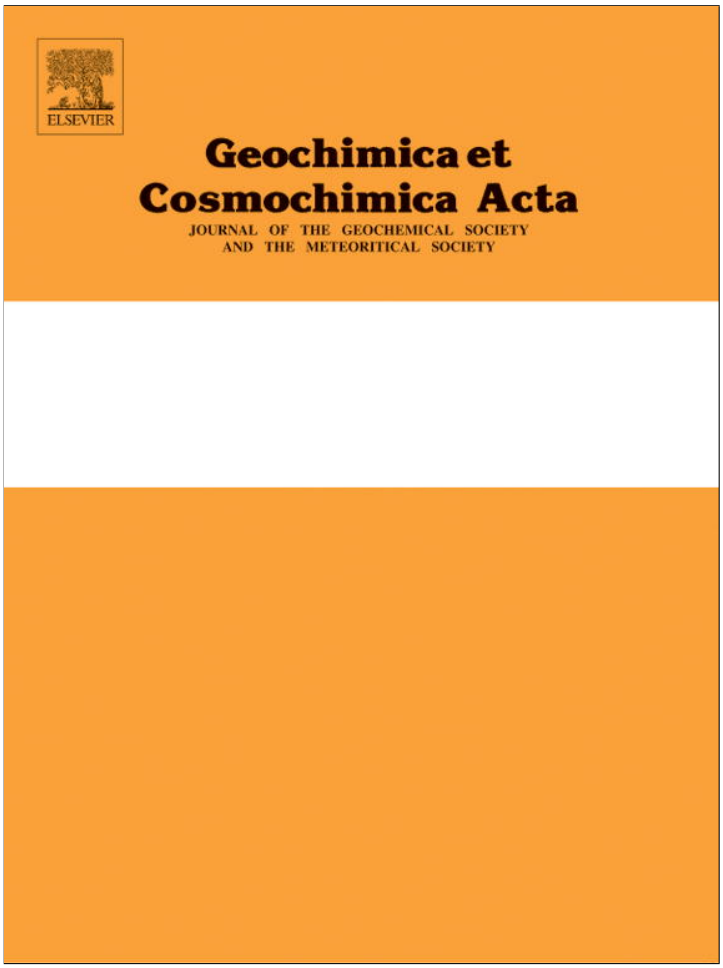

Available online at www.sciencedirect.com

SciVerse ScienceDirect

Geochimica et Cosmochimica Acta 110 (2013) 176–189

Geochimica et Cosmochimica Acta

www.elsevier.com/locate/gca

# Thermodynamic properties of aqueous $MgSO_4$ to 800 MPa at temperatures from −20 to 100 °C and concentrations to 2.5 mol $kg^{-1}$ from sound speeds, with applications to icy world oceans

Steve Vance *, J. Michael Brown

*Planetary Chemistry and Astrobiology, Jet Propulsion Laboratory, Caltech, United States*
*Earth and Space Sciences, University of Washington, Seattle, United States*

Received 4 May 2012; accepted in revised form 29 January 2013; Available online 11 February 2013

**Abstract**

Thermodynamic properties of aqueous magnesium sulfate solutions ($MgSO_4$ concentrations to 2.5 mol $kg^{-1}$) are reported in a previously unexplored regime of pressure and temperature. Solution densities (to a few hundred parts-per-million), specifics heats (to a few percent), and volumetric mixing parameters were determined to 800 MPa in the temperature range from −20 to 100 °C from sound speeds measurements. Equilibrium data extrapolate smoothly to temperatures below which liquids are stable, providing a basis for equilibrium freezing calculations. In more compressed water at high pressure, where electrostrictive effects are smaller, the partial molal volume at infinite dilution is positive and changes less with pressure, while the non-ideal contribution to the apparent molal volume is reduced. Ion–solvent and ion-ion contributions are small under all conditions, while solvent contributions to non-ideality show greater variation with pressure and temperature. In application to Ganymede, Callisto, and Titan, the current results suggest that concentrations of aqueous $MgSO_4$ would be exist that would be denser than overlying ice and thus buoyantly stable at the ice VI-rock interface, or between overlying layers of ice VI–V or V–III. More generally, the current data and analysis provide a comprehensive framework that can guide investigations of other single and multi-component aqueous systems.


## 1. INTRODUCTION

### 1.1. Background

The thermodynamic properties of aqueous $MgSO_4$ have been extensively investigated (Abdulagatov et al., 2007, and references therein). The conceptual framework developed by Pitzer (1973) for the general theory of aqueous solutions was originally explored using $MgSO_4$ in a set of monovalent and divalent ionic compositions. In combination with other common species, this chemical system is relevant for terrestrial studies ranging from the chemistry of seawater to chemical processes in hydrothermal systems. An understanding of processes occuring in icy moons in the outer solar system also requires knowledge of $MgSO_4$ thermodynamic properties (Vance and Goodman, 2009; Goodman and Lenferink, 2012). Missing in prior studies has been sufficient high pressure data to constrain this aqueous system under pressures relevant to planetary interiors (e.g., Marion et al., 2005).

Relevant pressures for oceans in large icy worlds, as shown in Fig. 1, range to 1000 MPa and higher if fluids penetrate into the lithosphere. The upper temperature range is relevant to hydrothermal systems and to ionic oceans in the interiors of Neptune and Uranus, and exoplanets of similar size and composition. Liquid water oceans inferred to exist

* Corresponding author. Address: MS 183-401, 4800 Oak Grove Drive, Pasadena, CA 91109, United States.
*E-mail address:* svance@jpl.nasa.gov (S. Vance).

0016-7037/$ - see front matter © 2013 Elsevier Ltd. All rights reserved.
http://dx.doi.org/10.1016/j.gca.2013.01.040

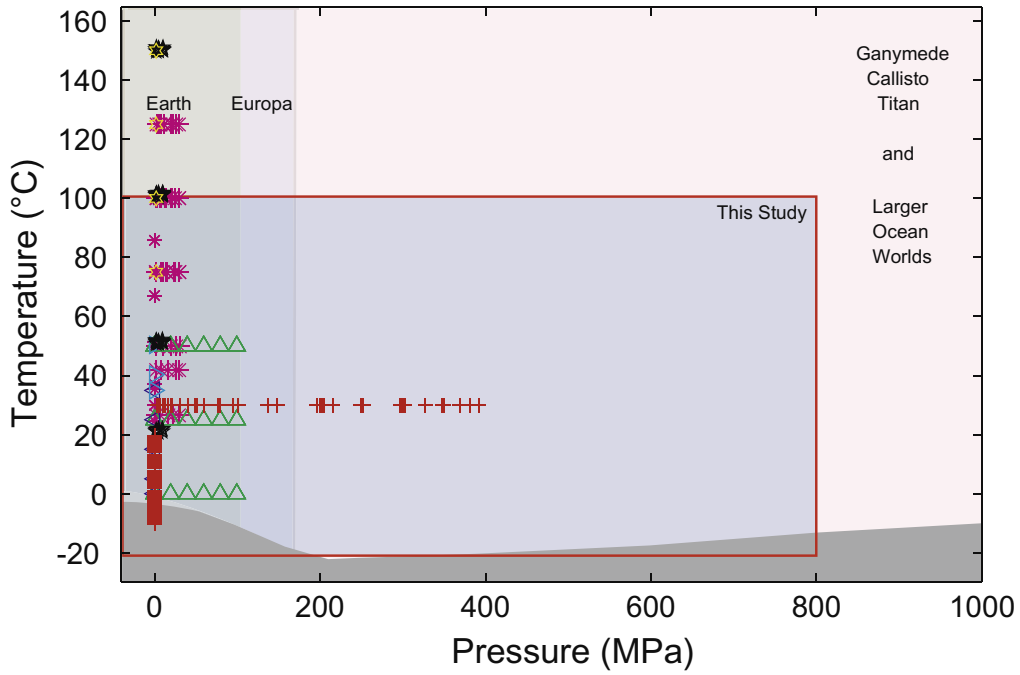


Fig. 1. Aqueous phase eqsuilibria, and a comparison between planetary regimes and experimentally accessible regimes of pressure and temperature. The darkly shaded region at the bottom denotes the range for the aqueous $MgSO_4$ system where no liquids exist, based on eutectic studies by Hogenboom et al. (1995) for $P < 400$ MPa; and Grasset et al. (2001), and Nakamura and Ohtani (2011) for higher pressures. The currently accessible range for laboratory studies is indicated. Plotted symbols are pressures and temperatures from prior determinations of densities in the aqueous magnesium sulfate system: ($^*$ Abdulagotov et al. (2007), + Hogenboom et al. (1995), five pointed star Phutela and Pitzer (1986a), six pointed star Phutela and Pitzer (1986b), triangle left Motin (2004), triangle up Chen et al. (1977), triangle left Chen et al. (1980)).

currently in Jupiter's icy moons Europa, Callisto, and, by inference, Ganymede (Khurana et al., 1998; Kivelson et al., 2009), and also in Saturn's moon Titan (Béghin et al., 2009, 2010; Iess et al., 2012) motivate further study of solution chemistry for plausible ocean compositions.

As documented in Fig. 1, densities for aqueous systems are scarce or non-existent at concentrations, temperatures and pressures relevant to subsurface aqueous reservoirs in icy worlds. There is a particular need for more work in the range of high salinity (concentrations greater than 1 mol $kg^{-1}$ in the $MgSO_4$ system) and in multi-component systems. Studies have partially addressed this problem (Hogenboom et al., 1995; Motin, 2004; Abdulagatov et al., 2007) but, until now, measurements at simultaneously low temperature and pressures above 100 MPa were non-existent.

We report thermodynamic properties for the aqueous magnesium sulfate ($MgSO_4$) system to 800 MPa, covering the majority of the range of liquid stability (area marked in Fig. 1) studied by Hogenboom et al. (1995), Grasset et al. (2001), and Nakamura and Ohtani (2011). Sound speeds as a function of pressure, temperature, and composition were measured by the method of impulsive stimulated scattering (Abramson et al., 1999; Abramson and Brown, 2004; Vance and Brown, 2010). From sound speed measurements, densities and specific heats were determined at high pressure. Volumes of mixing with respect to properties of water were determined using methods employed in previous studies (Abdulagatov et al., 2007).

### 1.2. Chemical thermodynamics of solutions

Given the specific volume of a solution, $V_{sp}$ (equal to the inverse of the solution density, $\rho_{sol}$), the volume that contains a kilogram of water is

$$V_s = (1 + 0.001mW)V_{\mathrm{sp}} \tag{1}$$

where $m$ is the molal concentration in mol $kg^{-1}$ and $W$ is the molecular weight of the solute in g $mol^{-1}$. Specific volumes are given here in mL $kg^{-1}$ and densities in kg $m^{-3}$. The solution volume, $V_s$ can be separated into the contribution from water plus ideal and excess volumes as

$$V_s = V_{\mathrm{water}} + mV^{\circ} + V_{\mathrm{excess}} \tag{2}$$

where $V^o$ is the partial molal volume at infinite dilution and the specific volume of water $V_{\mathrm{water}}$ has been well-studied. As a starting point, we use the equation of state from the International Association for the Properties of Water and Steam (Wagner and Pruss 2002) (hereafter referred to as IAPWS95) which reproduces a wide set of critically evaluated data (with fully characterized uncertainties) in the range of pressures and temperatures studied here. Our results include a slight modification of IAPWS95 at pressures above 500 MPa.

The framework for aqueous solution thermodynamics, using the partial molal volume for component $X$,

$$\bar{V}_{\phi,X} = \frac{\partial V_s}{\partial m_X} \tag{3}$$

expressed in a succinct form by Pitzer (1973) and further described elsewhere (e.g., Krumgalz et al., 2000), uses the dielectric properties of water to describe ion-water and ion-ion interactions in a manner that is consistent among different ions. This approach has been used to reproduce complex multi-species behavior in regimes of pressure, temperature, and concentration where experimental data are traditionally available (e.g., Wolery 1992; Marion and Grant 1994; Bethke 2008). The formulation of FREZCHEM described by Marion et al. (2005), which includes a linearized approximation to pressure behavior (further discussed below) and is optimized for subzero temperatures, is used herein as a basis of comparison with the current work and the relevant literature.

A quantity reported in experiments, the apparent molal volume $\phi_v$, is defined as:

$$\phi_V = \frac{(V_s - V_{\text{water}})}{m} \tag{4}$$

where $\phi_v$ has units of mL mol$^{-1}$. Following standard solution chemistry analysis (e.g. Abdulagatov et al., 2007), $\phi_v$ at each pressure and temperature can be represented as the sum of ideal and excess terms:

$$\phi_v = V^0 + m^{1/2}V_{dh} + mV_b + m^{3/2}V_d \tag{5}$$

where the excess contribution includes the infinite dilution limiting slope of the Debye-Hückle contribution (with coefficient $V_{dh}$) and two additional terms (coefficients $V_b$ and $V_d$) that are proportional to higher powers in concentration. Within the solution chemistry framework (Krumgalz et al., 2000; Marion et al., 2012) $V_b$ is often associated with ion–solvent interactions and $V_d$ represents ion-ion interactions.

## 2. METHODS

### 2.1. Laboratory experiments

Using previously described instrumentation (Vance and Brown 2008; Vance and Brown 2010) sound speeds were measured (with a nominal reproducibility of about 0.2%) as a function of pressure (absolute accuracy of 0.7 MPa) and temperature (controlled to 0.1 °C) by impulsive stimulated scattering (Abramson et al., 1999). Fluid samples of varying composition were prepared by measuring high purity de-ionized water (de-aerated by vacuum) into large volumetric graduated (to 1 mL) flasks. Masses (measured to a 0.1 mg) of ultra-pure (HPLC-grade) hydrated magnesium sulfate ($MgSO_4{\cdot}7H_2O$), the stable phase under standard conditions, were added, accounting for stoichiometric water in the hydrated solid. The uncertainty of resulting fluid concentrations is estimated to be better than 0.001 mol kg$^{-1}$.

Measured sound speeds in de-ionized water (previously reported in Vance and Brown, 2010 and included in the Supplemental materials for convenience) and in aqueous $MgSO_4$ at concentrations of 0.080, 0.510, 0.997, 1.506 and 2.014 mol kg$^{-1}$ are given in the Supplemental tables. Measurements are consistent with literature values (Millero and Chen 1985; Millero et al., 1987) at low pressure for all temperatures. Sound speeds measured in separate runs were reproducible within experimental limits despite a varying history of pressure and temperature cycling for individual sample loads.

The true acoustic absorption in these experiments was smaller than our ability to quantify it. Either slow structural relaxation in water or slow relaxation of ion-pairing equilibrium would introduce error in the analysis. The relaxation frequencies of simple diffusion-controlled reactions are, however, in these concentrated solutions, expected to be larger than the experimental frequencies. It seems likely that an equilibrium sound speed is measured.

### 2.2. Determining the thermodynamic state surface

A description spanning a broad range of thermodynamic states is needed of the Gibbs energy surface (and properties based on derivatives of Gibbs energy including specific heat, volume/density, thermal expansivity, and sound speed). Researchers seeking to accurately represent these surfaces have used increasingly sophisticated formulations (see Span 2000). In the case of water, an adequate representation (IAPWS95) required 58 analytic and non-analytic functions that were manually selected from a library of several hundred possible terms. Key in this work was the inclusion of basis functions that contribute in a restricted range of pressure and temperature. The resulting (more localized) description is thus less weighted by data far from a specified point.

Here, distinct from other equation of state formulations, in which a complex equation is adapted to suit features of a specific data set or may contain theoretical assumptions about how the surface should behave, we describe the thermodynamic state surface as values on a grid in pressure, temperature and composition. The grids are sufficiently dense to allow interpolation. All reported thermodynamic properties are internally consistent; derivatives and integrals based on interpolation of the tables obey fundamental thermodynamic cross relationships.

Earlier work by Wiryana et al. (1998), Abramson et al. (2001), Abramson and Brown (2004), Vance and Brown (2010), Lin and Trusler (2012) shows that solutions to a numerical forward problem, based on measured sound speeds at pressure and temperature, give accurate densities at high pressure. The coupled equations in this calculation are:

$$\left(\frac{\partial \rho}{\partial P}\right)_T = \frac{1}{v^2} + \frac{T\alpha^2}{C_p} \tag{6a}$$

$$\left(\frac{\partial C_P}{\partial P}\right)_T = -T\left(\frac{\partial^2 V_{sp}}{\partial T^2}\right)_P \tag{6b}$$

where $v$ are the sound speeds, $\alpha$ is thermal expansivity, $C_p$ is specific heat, and density $\rho = 1/V_{sp}$ where $V_{sp}$ is the specific volume. The constants of integration are given by values of density and specific heat at one pressure (typically 0.1 MPa).

The specific volume (as a function of pressure, temperature and composition) is found in an inverse calculation such that resulting sound speeds, determined through the

appropriate derivatives of that surface, match measurements. The surface is parameterized using splines as described by de Boor (2001) so that values and derivatives of the surface are evaluated analytically. Using regularized (Tikhonov) inversion (Aster et al., 2012), a smooth surface is found that adequately fits measurements. The trade-off between data misfit and surface smoothness is adjusted such that mistfit is consistent with expectations based on experimental uncertainties and observed trends of data with respect to pressure, temperature and concentrations are adequately reproduced by the fit.

Using standard inverse techniques (Aster et al., 2012), uncertainties due to random experimental errors were determined on the basis of an ensemble of 100 inversions using synthetic data. Sound speeds were calculated at the pressure–temperature-composition points of the actual data and random noise with a variance of 0.25% was added. Each synthetic data set was inverted (changing the random noise with each attempt) to give the state surfaces and all solution chemistry properties. $3\sigma$ deviations of the ensemble results for the properties are reported as maps of uncertainty in pressure and temperature.

Several advantages are associated with the current approach. Values and their uncertainties are determined using widely adopted and standardized inverse techniques. Arbitrary numerical precision is obtained through appropriate choices for grid spacing and spline order. Other data, in addition to sound speeds, can be straightforwardly assimilated within this inversion framework. The task to find or revise the state surface in the face of new or revised data is easily accomplished.

In terms of application in geochemical modeling, complex analytic formulations (or those not parameterized with pressure as an independent variable) are often pre-processed into look-up tables to speed calculations. Computer implementation of our results is straightforward since we provide tables that can be directly interpolated. More generally, since digital database implementations and tools are now universal, we see no disadvantage associated with either a digital representation that contains more parameters than does a traditional equation, or the need for computer-based tools to access this representation.

### 2.3. Integration constants

The required initial densities and specific heats at 0.1 MPa at all temperatures for pure water are based on IAPWS95. Primary data sources for densities of the $MgSO_4$ solutions at 0.1 MPa at all temperatures are reported and evaluated in several reports (e.g., Monnin 1989; Marion et al., 2005). Uncertainties for the data of Millero and Knox (1973), Chen et al. (1977), Lo Surdo et al. (1982), Millero and Lampreia (1985), Phutela and Pitzer (1986a,b), and Millero et al. (1987) are reported to be a few tens of parts per million (ppm). Abdulagatov et al. (2007) reported uncertainties of 600 ppm for data that extend to higher temperatures. The only experimental constraints on densities in the sub-zero temperature range (Hogenboom et al.1995) have larger errors, estimated to be near 1000 ppm (0.1%). A smooth density surface in temperature and composition was fit to selected data within the reported uncertainties. Specific heats of the solutions were estimated from ionic contribution to the specific heat at infinite dilution using the slop92 database (Johnson et al., 1992). For temperatures below 0 °C, the ionic contribution was approximated by extrapolation. We determined by calculation that large changes in the approximations for specific heats of the solutions at 0.1 MPa have negligible impact on our results.

### 2.4. Surface state uncertainties

Since all thermodynamic properties derived in this work are anchored to literature data at 0.1 MPa, the contribution here is in the determination of changes in those properties at elevated pressures. Uncertainties therefore increase with increasing pressure. Based on uncertainty maps, 800 MPa was chosen as the highest pressure of our grid and 2.5 mol $kg^{-1}$ was chosen for the highest concentration. These relatively modest extrapolations from the range of data are justified by the relatively smooth and nearly constant derivatives of sound speed at the highest pressures, and for higher concentrations, which lead to slow growth in uncertainty even beyond the regime of measurement.

Experimental data are non-existent where water and $MgSO_4$ (aq) are metastable relative to ice at low temperature and high pressure. The sound speed surface in this metastable range is an estimation based on a plausible smooth extrapolation from regimes sampled by measurement. In spite of the larger uncertainties in this regime, we report values (with well characterized uncertainties) in order to provide a continuous thermodynamic surface that is necessary to describe solution properties over the widest possible range of concentration.

### 2.5. Determination of mixing properties

Apparent molal volumes were calculated as in Chen et al. (1977). Following common practice, (e.g., Motin 2004) we determined the partial molal volume at infinite dilution, $V^o$, by extrapolation of $\phi_v$ to zero concentration as a function of $m^{1/2}$. The remaining parameters in Eq. (5) ($V_{dh}$, $V_b$ and $V_d$) were determined by least-square fitting of the difference ($\phi_v - V^o$) as a function of concentration at each gridded point of pressure and temperature.

## 3. RESULTS

A surface for volume as a function of state variables is the primary analysis product. Tables of values as a function of pressure temperature and concentration are given in the Supplemental materials. State surface properties for specific heat, thermal expansivity, and sound speeds are inherent in the shape of the volume surface. For convenience we report derivative values in separate tables. Properties under non-tabulated conditions can be adequately determined by interpolation of these tables. Separately, we report mixing coefficients, based on Eq. (5), that presumes validity of a particular framework for solution thermodynamics. In the discussion section we present several graphical projections of the state surfaces to illustrate our findings.

## 4. DISCUSSION

### 4.1. Experimental data

#### 4.1.1. Sound speeds

Since sound speeds are the primary high pressure data, only in this case is it possible to make detailed comparisons over the entire regime of pressure, temperature, and composition between data and a thermodynamic state surface representation. In Fig. 2, the left panel shows measured sound speeds and state surface isotherms versus pressure. In the middle panel the same data and state surface isobars are plotted on the temperature axis. In the right panel deviations of sound speeds from the state surface representation of sound speeds are plotted versus pressure. The six compositions are offset vertically in each panel.

The overall *rms* misfit between data and the sound speed state surface of 0.25% was chosen in the inverse problem through adjustment of smoothing parameters. Smaller misfit (less smoothing) resulted in implausible structure of the representation to more closely follow data. With greater smoothing, systematic misfit of data resulted. That misfits of data show no clear systematic behavior and are consistent with laboratory estimates of experimental uncertainty is evidence that this state surface representation is satisfactory.

Expected trends of sound speeds with respect to pressure, temperature and composition are apparent. Pressure derivatives decrease at high pressure. Temperature derivatives are modest and decrease with concentration and with pressure. The effect of increased concentration depends on the pressure. Almost no dependence of sound speed with concentration is observed at the highest pressures where values converge on approximately 2.6 km $s^{-1}$ at 800 MPa.

#### 4.1.2. Density, thermal expansivity, and specific heat

Three projections in concentration of thermodynamic state surfaces for densities (upper panels), thermal expansivity (middle panels) and specific heat (lower panels) are shown in Fig. 3. On the basis of Eq. (6) larger first and second derivatives of density with respect to temperature lead to larger changes of both thermal expansivity and the pressure dependence of the specific heat. General trends of the properties displayed in the figure are as expected since the sound speed surface has larger temperature and pressure gradients at low pressure.

Comparisions are shown in Fig. 3 between data and published formulations (IAPWS95 for pure water and FREZCHEM for solutions). Although deviations in density are small, our results differ from IAPWS95 in a regime above about 500 MPa where little data constrained that work. Deviations from FREZCHEM are larger at high pressure

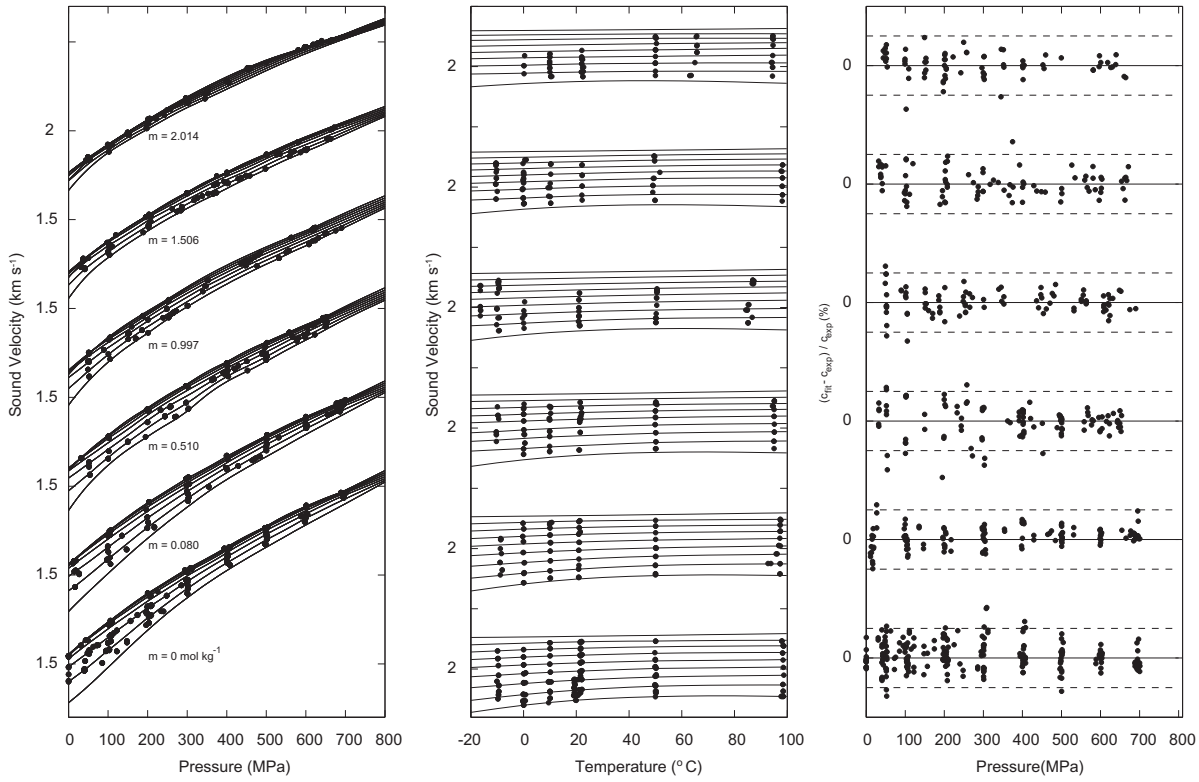


Fig. 2. Speeds of sound in aqueous $MgSO_4$ to 800 MPa from −20 to 100 °C for six compositions. Solid symbols are data and lines are projections of the thermodynamic state surface. In the left panel, tick marks are separated by 0.5 km $s^{-1}$ and each compositional set is plotted relative to a sound speed marker at 1.5 km $s^{-1}$. In the middle panel, tick marks are separated by 1 km $s^{-1}$ and each compositional set is plotted relative to a sound speed marker at 2 km $s^{-1}$. In the right panel percentage residuals between measured sound speeds in aqueous $MgSO_4$ and the state surface are plotted versus pressure for the six concentrations. Dashed lines are ±0.5%.

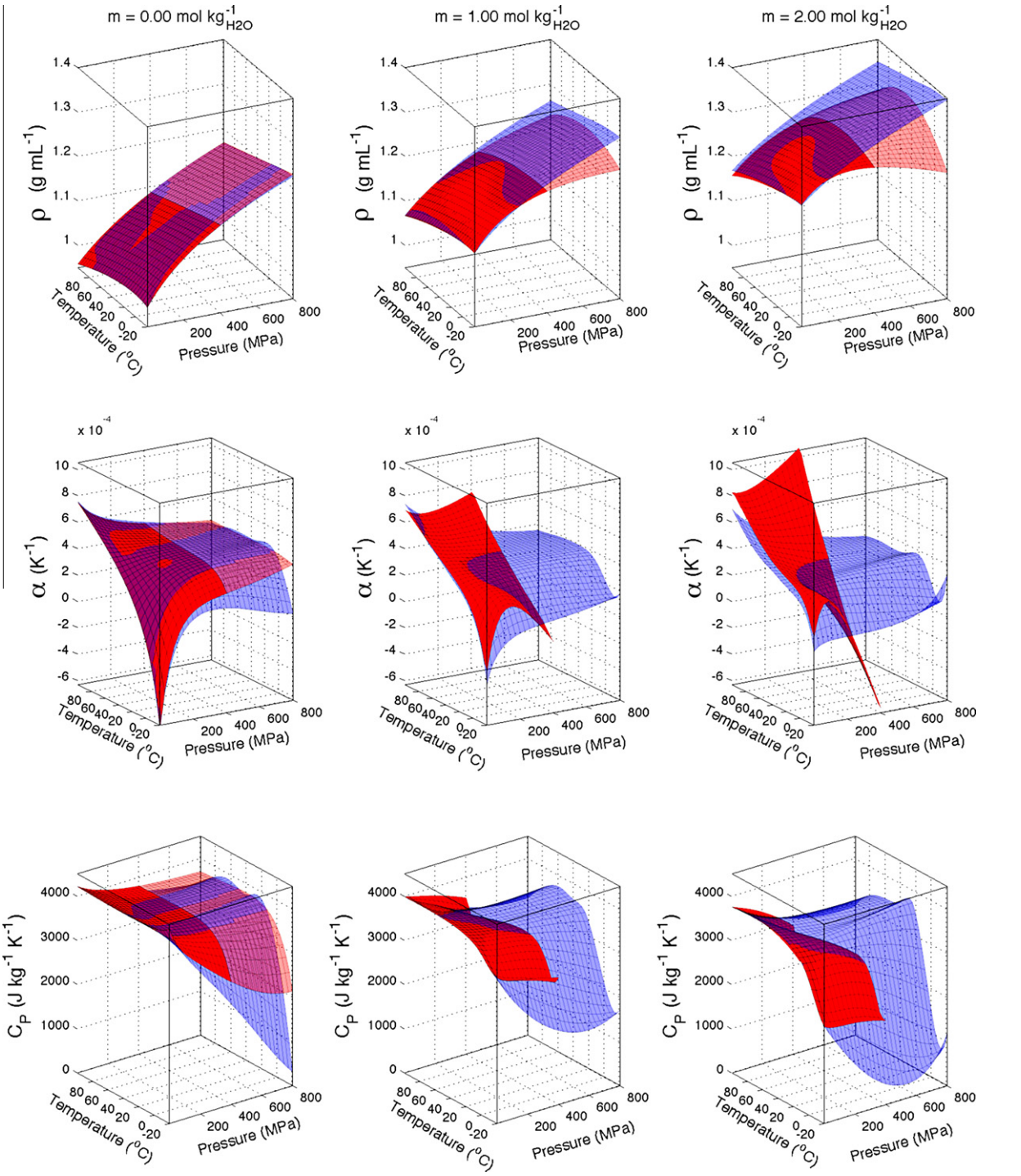


Fig. 3. Projections of the thermodynamic state surfaces for density (upper), thermal expansivity (middle), and specific heat (lower), as a function of pressure and temperature. Left panels: water. Middle panels: molal concentration of 1 mol $kg^{-1}$. Right Panels: molal concentration of 2 mol $kg^{-1}$. Blue shaded surfaces are current results. Red shaded surfaces are IAPWS for water and FREZCHEM for solutions. The lighter shadings represent regimes in which FREZCHEM (upper panel only) has been extrapolated well beyond the data that underly its formulation and in which fewer data constrained IAPWS.

where assumptions made by Marion et al. (2005) are likely to fail (as discussed below). The limited and lower pressure determinations of solution densities reported by Hogenboom et al. (1995) and Abdulagatov et al. (2007) are in accord with our results within their reported uncertainties.

Uncertainty maps at the $3\sigma$ level associated with state surface projections in Fig. 3 are given in Fig. 4. The density of water is determined to about 100 ppm to a pressure of 800 MPa. Uncertainty for the more concentrated solutions are about twice as large. Thermal expansivities and specific

heats above 500 MPa are uncertain at the level of several percent. The temperature dependence of the uncertainties are generally small with the exception of the metastable regime near 800 MPa and −20 °C where results are based on extrapolation and the errors become significantly larger.

### 4.2. Interpretation of the results

#### 4.2.1. Mixing coefficients, ideal and excess properties

The state surfaces described previously depend only on measurement. The discussion in this section depends on a particular theoretical framework. In Fig. 5 the four mixing coefficients ($V^o$, $V_{dh}$, $V_b$, and $V_d$) of Eq. (5) are shown as a function of selected pressures (0.1, 100, 200, 400 and 800 MPa) and at all temperatures. The ensembles of synthetic results are plotted in a lighter shade to provide a visual indication of uncertainty (the spread of these estimates is approximately equal to a 2σ error estimate).

To the extent that the four parameters in Eq. (5) are associated with a fundamental theory (e.g., Krumgalz et al., 2000), the values have physical significance. In particular, the first term, $V^o$, gives the ideal contribution to the volume of mixing. It is the largest term, shows the most variation with pressure and temperature, and is further discussed be-

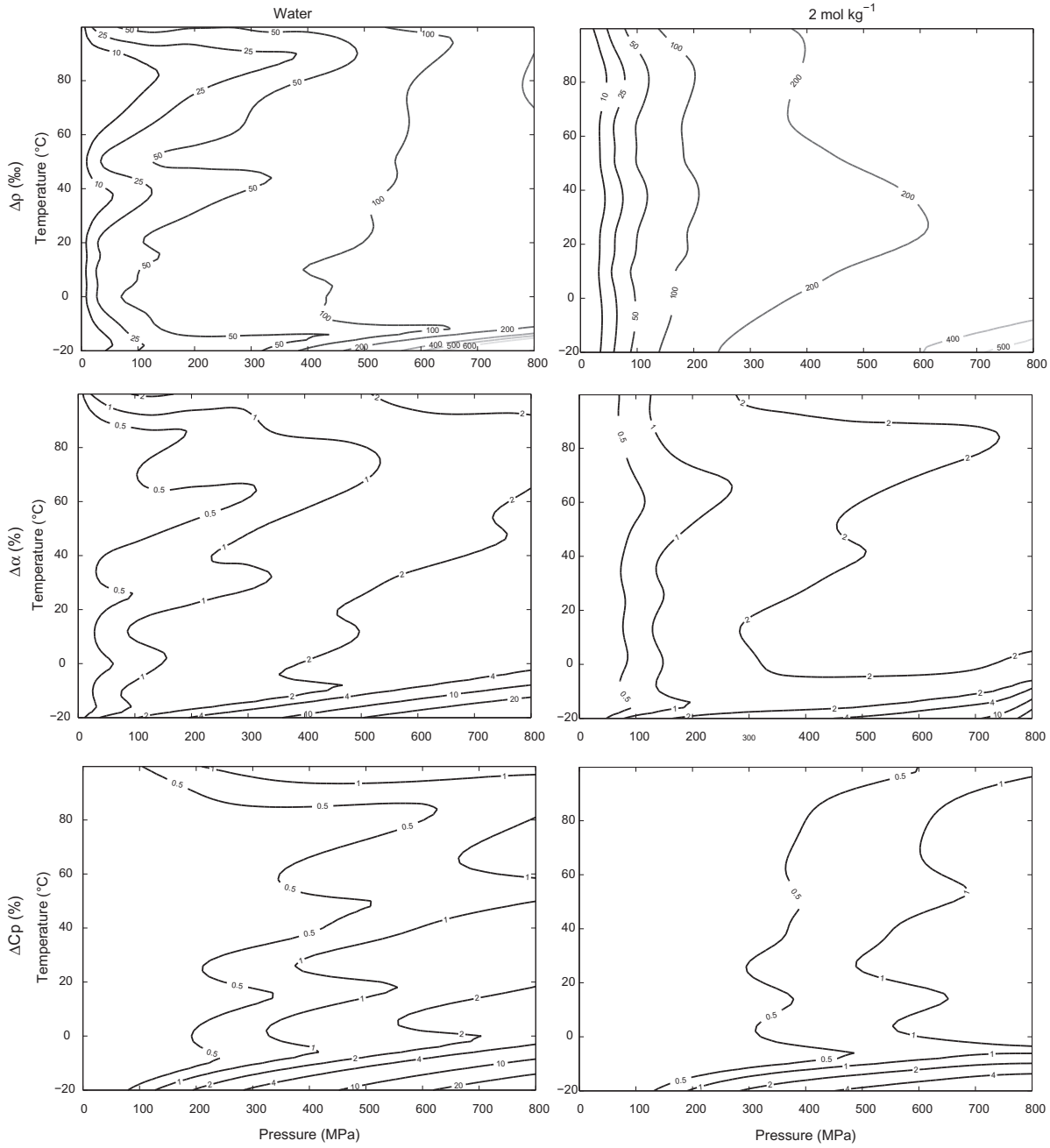


Fig. 4. Projections of uncertainty maps at the 3σ (99%) confidence level for density (upper), thermal expansivity (middle), and specific heat (lower), as a function of pressure and temperature. Left panels: water. Right panels: molal concentration of 2 mol kg$^{-1}$.

low. The second term, $V_{dh}$, the limiting slope of the Debye-Hückel contribution to the excess volume, is also large and has clear trends that are not matched by standard estimates (dashed lines) as discused further below. In contrast, the last term, $V_d$, associated with ion-ion interactions, is small relative to the other terms and exibits little dependence on pressure and temperature while $V_b$, the ion–solvent interactions, is slightly larger and has a pressure dependence larger than uncertainty only at the higher temperatures.

In Fig. 6a apparent volumes for a concentration of 1 mol kg$^{-1}$ are compared with ideal and excess contributions Eq. (2). The general trend is for the excess contribution to decrease with pressure. At 800 MPa $V_{excess}$ gives about 25% of the total apparent volume. A large temperature dependence, exhibited at 0.1 MPa for all surfaces, is reduced at high pressure except in the high pressure metastable regime at the lowest temperatures.

In Fig. 6b the present partial molal volumes at infinite dilution are compared with predictions from Marion et al. (2005) and with the accumulated measurements at 0.1 MPa presented by Abdulagatov et al. (2007). The broad range of ambient pressure experimental values underscores the difficulty in accurately determining $V^o$ for magnesium sulfate. Phutela and Pitzer (1986b) noted that that the slope of $\phi_v$ with concentration is much steeper for $MgSO_4$ than for other electrolytes. They chose to infer $V^o$ indirectly based on measurements in other solutions, namely: $V^0_{MgSO_4} = V^0_{MgCl_2} + V^0_{Na_2SO_4} - V^0_{NaCl_4}$. Our determination of $V^o$ at 0.1 MPa follows the predictions of Marion et al. (2005) in the low temperature regime and follows the trend of the more recent high temperature data found in the analysis by Abdulagotov et al. (2007). The large negative value of $V^o$ is a result of a large electrostrictive effect of these ions on the structure of uncompressed water.

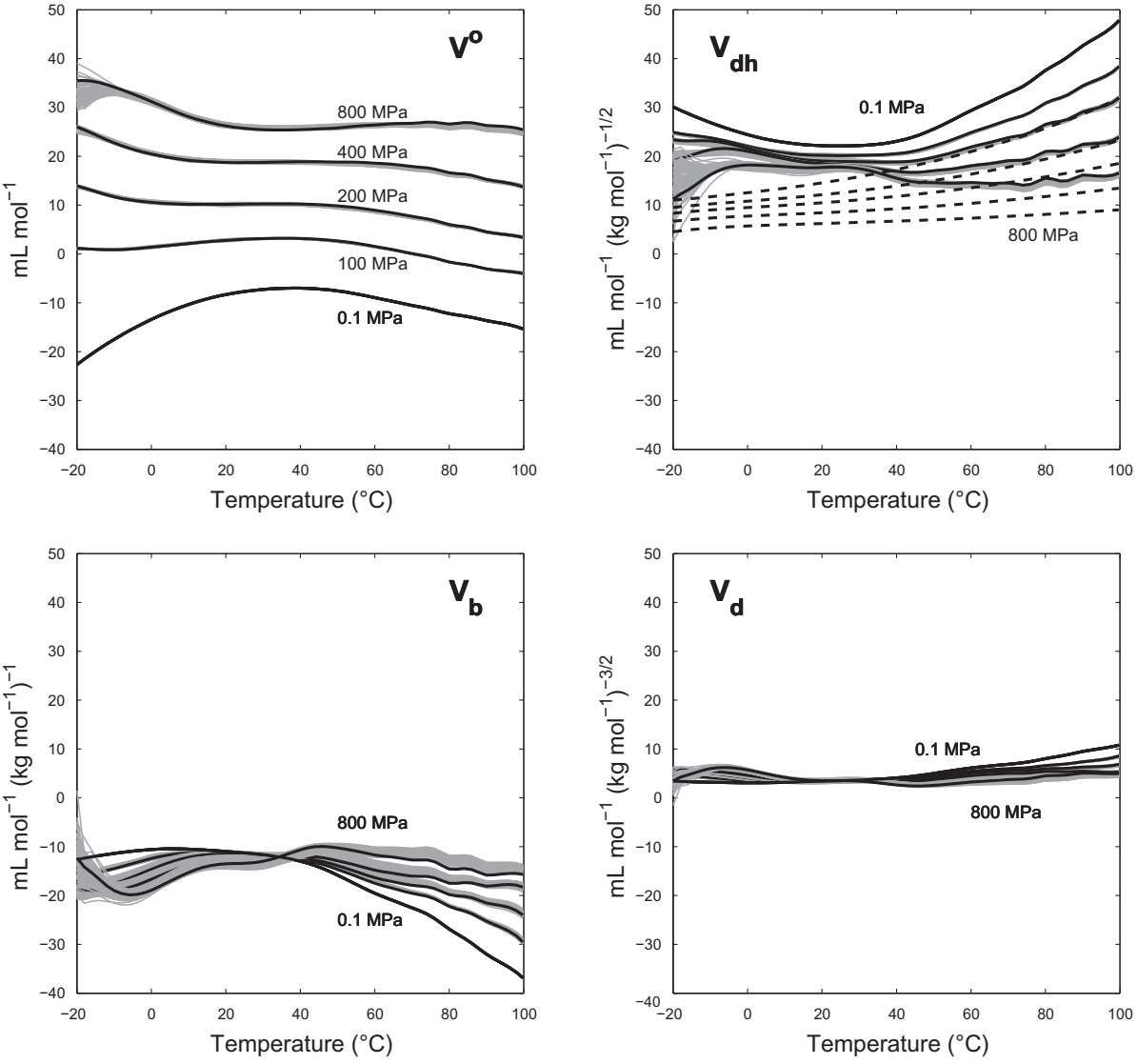


Fig. 5. Mixing parameters ($V^o$, $V_{dh}$, $V_b$, and $V_b$) for $MgSO_4$ as a function of temperature. In each panel, the solid black line are isobaric projections. The lighter gray shading gives an estimate of uncertainty (2σ) for each parameter. Dashed lines in the $V_{dh}$ panel are theoretical estimates for the limiting slope Debye-Hückel contribution.

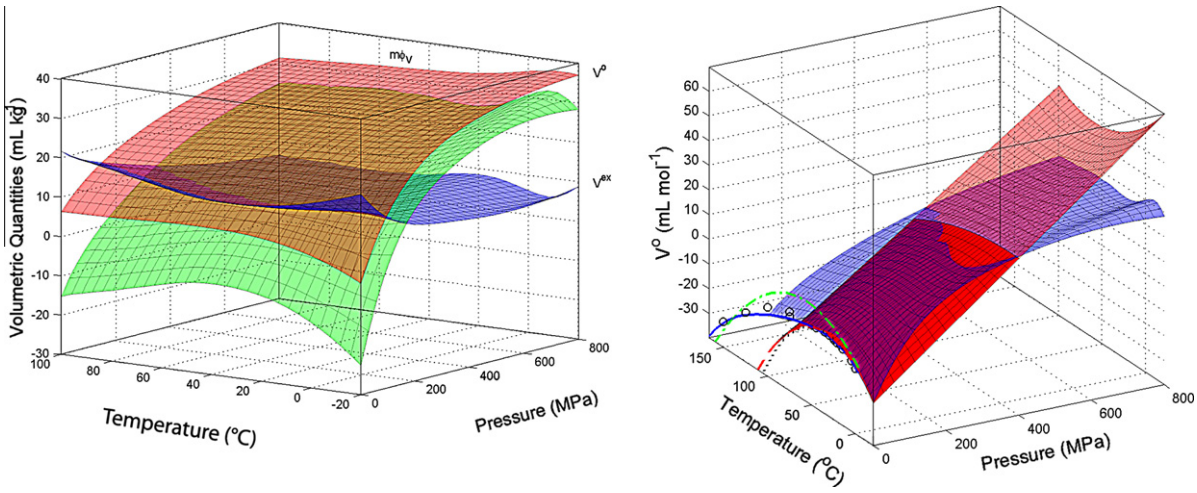


Fig. 6. Surfaces in pressure and temperature of the apparent and partial molal volumes of aqueous $MgSO_4$. Left panel: The apparent molal volume at a concentration of 1 mol $kg^{-1}$ and its ideal and excess components. Right panel: Partial molal volumes at infinite dilution. Data (circles) and 0.1 MPa curves are from Abdulagotov et al. (2007). Solid surface to 400 MPa and extended with transparancy to 800 MPa is based on the pressure and temperature dependence given in FREZCHEM. The remaining surface (upper at low pressure and lower at high pressure) is the current result.

In past work on electrolyte chemistry (Krumgalz et al., 1999; Marion et al., 2005) for pressures below 100 MPa, partial molal volumes at infinite dilution were calculated as $V^o(P,T) = V^o(P = 0.1,T) - \kappa^o(T)\Delta P$, with the compressibility term $\kappa^o$ assumed constant in pressure (Millero, 1983). At pressures above 200 MPa our results indicate that the compressibility term becomes substantially smaller. This is expected since electrostrictive effects in more compressed water are reduced and the ions are relatively incompressible. The impact of an inappropriate linear extrapolations of $V^o$ to higher pressures is clearly shown in Fig. 3, where FREZCHEM predictions for density unphysically decrease with increasing pressure.

The dashed (isobaric) lines in the $V_{dh}$ panel of Fig. 5, were calculated from the slope at infinite dilution of the Debye-Hückel function (Fernandez et al., 1997). The data underlying the parameterization of the dielectric constant, needed to calculate the Debye-Hückel contribution, extend to only 500 MPa and at sub-zero temperatures were restricted to 0.1 MPa. To the extent that smooth extrapolations of the dielectric constant are appropriate, it would appear that our determination of $V_{dh}$ follows theoretical expectations for the pressure dependence better at temperatures above room temperature. At 0.1 MPa and for temperatures below room temperature, the deviation of $V_{dh}$ from the theory is a robust experimental feature required by the increasingly negative values of $V^o$. The pressure dependence of $V_{dh}$ at low temperature is clearly inconsistent with the estimate based on smoothly extrapolated behavior of the dielectric constant.

The relationship between the fitted coefficient $V_{dh}$ and Debye-Hückel behavior is complicated by ion-pairing behavior as a function of pressure and temperature. Application of the standard expression for the Debye-Hückel limiting slope assumes that aqueous $MgSO_4$ is dissassociated (consisting predominantly of $Mg^{+2}$ and $SO_4^{-2}$ ions). A body of experimental work based on both electrical conductivity measurements (Madekufamba and Tremaine, 2011 and references therein) and on interpretation of Raman scattering lines shapes (Frantz et al., 1994) has shown that at relatively low pressures and at high temperatures, $MgSO_4$ becomes increasingly associated. In the work of Frantz et al. (1994), this sytem was reported to be nearly fully associated at 500 °C and 1100 MPa. This outcome is likely caused by the decrease in the dielectric constant of water at high temperature. Based on changes in the dielectric constant with pressure and temperature (Fernandez et al., 1997), $MgSO_4$ should be more fully ionized at high pressures and at low temperatures and should be more associated at high temperatures and low pressures. Deviations of the coefficient $V_{dh}$ from the dashed curves in Fig. 5 are not fully in accord with this interpretation.

#### 4.2.2. Extension to multi-component systems

The present work provides a data collection and analysis framework that serves as a guide for investigations of other single aqueous species and can be extended to consideration of multi-component systems. We report fitted mixing coefficients that are, within the solution chemistry framework, determined from appropriate sums of contributions of the individual ion species ($Mg^{+2}$ and $SO_4^{-2}$). If the same coefficients are determined for other aqueous solutions (NaCl, $MgCl_2$, $Na_2SO_4$, and more) and if the theoretical framework remains valid over the entire thermodynamic space, determination of all individual anion and cation contributions to the high pressure behavior should be possible (e.g., Millero and Chen, 1985; Badarayani et al., 2000; Krumgalz et al., 2000; Hu and Fan, 2001; Hu, 2001; Denisov et al., 2003, 2004, and Denisov, 2007). This will enable a more robust ability to predict high-pressure equilibrium chemical processes. The thermochemical data provided here extrapolate smoothly below known liquidus temperatures, providing a basis for equilibrium freezing calculations. Marion et al. (2005) found that extrapolation of equilib-

rium volumetric properties for pure water below freezing provided FREZCHEM with predictive capabilities for the freezing of multicomponent solutions, more accurate than measurements in supercooled fluids.

*4.2.3. Applications to icy satellite geology and interior processes*

Deep (100 km) subsurface oceans in icy satellites like Europa, Ganymede, Callisto, and Titan can occupy a substantial portion of satellites volumes (e.g., Hussmann et al., 2006; Vance et al., 2007), constituting significant thermal mass. It has been suggested that water's anomalous thermal expansion properties (Melosh et al., 2004) or double-diffusive convection (Vance and Brown, 2005) might serve as a means for storing heat in Europa's ocean. The current set of thermodynamic properties can be used to accurately model such activity.

The extremes of pressure explored in our laboratory are encountered in high-pressure ice layers at the bottoms of oceans in the largest icy satellites, Ganymede, Callisto, and Titan. Analogies to Earth's seafloors are difficult to draw for these objects, as liquid–water hydrothermal activity would seem to be largely precluded where the ocean is sandwiched between ice layers. Densities for aqueous magnesium sulfate can, in principle, exceed those of high pressure ice phases owing to higher compressibility, as illustrated in Fig. 7 based on equations of state for ice phases from Choukroun and Grasset (2010). There exists an intermediate range of concentrations for aqueous $MgSO_4$, in which fluids are buoyant in the denser ice VI phase, but not in the less dense ice V phase that would lie above the ice VI layer. Likewise, there exists a less saline regime of fluids that are buoyant relative to an ice V layer denser than an overlying layer of ice III. One might envision the existence, therefore, of a layered ocean–colloquially, a "Dagwood sandwich" ocean–for these larger satellites, with distinct liquid water layers. An example is shown for Ganymede in Fig. 8, using mean $H_2O$ layer thickness from Anderson et al. (1996) and relative ice layer thicknesses from Barr et al. (2001). We note that the ice III

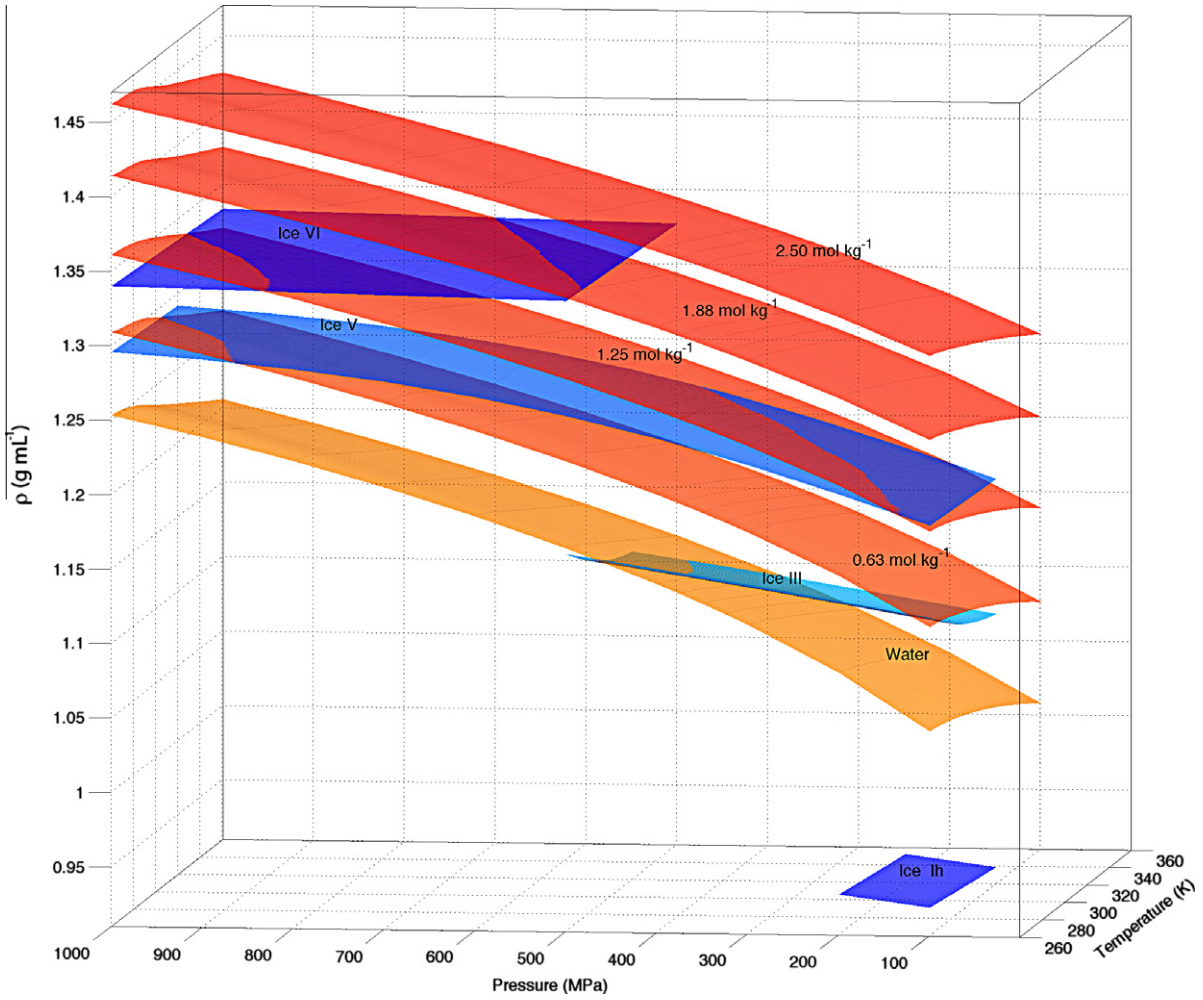


Fig. 7. Densities of concentrated $MgSO_4$ solutions compared with those of ice I and high-pressure ice phases III, V, and VI in the range of pressure and temperatures explored in this work. Ice III is less dense than ice V, which is less dense than ice VI. Ice I is less dense than liquid phases at all pressure and temperatures. All solid phases are less compressible than the fluids, which increase in density with increasing pressure and concentration.

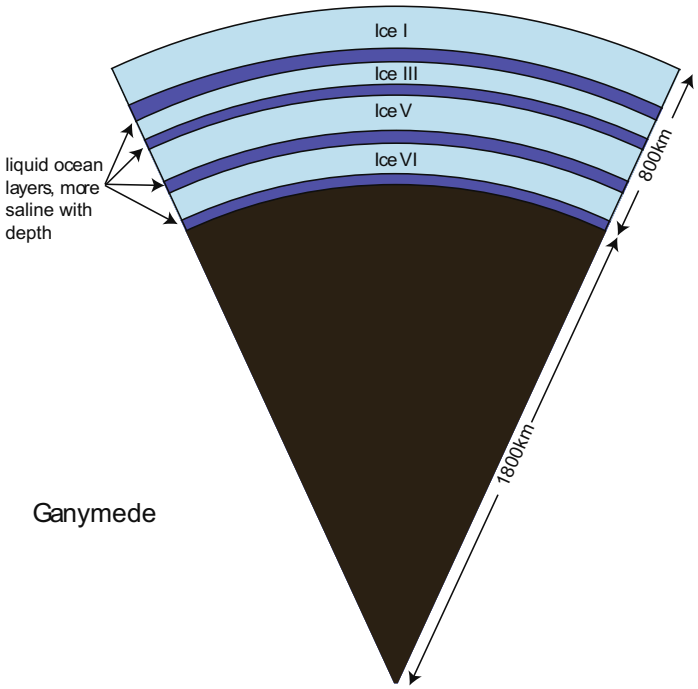


Fig. 8. A hypothetical "Dagwood sandwich" structure for Ganymede or other large icy worlds. Gravitationally stable layers of ice are illustrated with intervening liquid saline layers separating the high pressure phases of ice. (Based on the density relationships in Fig. 7).

layer pictured therein can co-exist with the main ocean only in a narrow regime of heat flow (e.g., Sotin and Tobie, 2004). Callisto and Titan, which are also thought to contain liquid water, are similar in size and could also conceivably host multiple ocean layers. If present, such a feature might be observed in seismic and induced magnetic field signatures by future landed robotic exploration missions. The mechanical and thermodynamic evolution of putative oceans underlying high-pressure ice layers has not been explored; perched ocean layers would be transient unless steady-state thermal profiles within the oceans lie near the melting phase boundaries. One previous study by Barr et al. (2001) investigated pure water melt intrusion into Ganymede's (upper) ocean by volcanism, but did not consider the effects of salinity on buoyancy.

The current results for the aqueous $MgSO_4$ system should allow better assessment of geophysical signatures between highly saline and pure-water oceans that might be measured in future exploration missions, such as the Ganymede orbiter planned by the European Space Agency (Dougherty et al., 2012). Sound speeds for concentrated $MgSO_4$ approach shear velocities for water ice I (Gagnon et al., 1990), differing from sound speeds in pure water by as much as 30%. In evaluating seismic studies of Europa's interior, Lee et al. (2003) suggest that contrasts in seismic structure on the order of 10% would be detectable by a single surface hydrophone. The absence of shear modes in aqueous $MgSO_4$ would clearly dilineate trapped pockets of concentrated fluid; the similarity in sound speeds in ice and brine would complicate location of relevant features but would not make the problem intractable. Large-scale density variations in Europa's ocean (or in that of Enceladus) due to upwelling hydrothermal features or downwelling intrusions from the ice shell, for example, can be modeled in this context using the thermodynamic data provided here.

## 5. CONCLUSION

Thermodynamic state surfaces (density, thermal expansivity, sound speeds, and specific heat) for concentrated aqueous solutions of $MgSO_4$ are reported covering a previously unexplored regime of pressure and temperature. A new framework for sound speed data collection and analysis based on the local representation of thermodynamic state surfaces determined through standard inverse methods should be generally applicable in other studies of solution properties. The laboratory data extend to a concentration of 2 mol $kg^{-1}$ in a temperature range from −20 °C to 100 °C and to a pressure of 700 MPa. Sound speeds are fit to a *rms* error of 0.25% which is consistent with estimated laboratory uncertainty. Based on the slow growth of uncertainties in an extrapolated regime (as a result of nearly linear behavior for sound speeds at high pressure and for concentrated solutions) thermodynamic properties are reported to 800 MPa and for concentrations to 2.5 mol $kg^{-1}$. Uncertainties in the reported properties increase with increasing pressure since results are anchored to literature values at 0.1 MPa. Nominals density uncertainties at 800 MPa lie in the range of several hundred parts per million. Uncertainties in thermal expansivities and specific heats at the highest pressures lie in the range of several percent.

Volumetric mixing parameters are determined using conventional analysis. Partial molal volumes at infinite

dilution (the ideal mixing contribution) are large and negative at low pressure where electrostrictive effects of ions on water are largest. Partial molal volumes are large and positive at higher pressures where electrostriction on already compressed water is less effective. In this regime, the greater incompressibility of ions results in a reduced pressure dependence for the partial molal volume. Non-ideal contributions to the volumes of mixing decrease with pressure. At 800 MPa the excess volume is about 25% of the apparent volume. The largest non-ideal contributor, the Debye-Hückel term is reduced at high pressure as a result of the increasing dielectric constant of water (e.g. Bradley and Pitzer, 1979). Fitted coefficients, associated in theory with ion–solvent and ion-ion interactions, show less dependence on pressure and temperature and provide a small but non-negligible contribution to excess properties. The effect of changes in the disassociation/association of ions as a function of temperature and pressure on the solution chemistry framework, where full disassociation is presumed, remains to be resolved.

In application to Ganymede, Callisto, and Titan, the current results suggest that, based on buoyancy relative to ice, a $MgSO_4$-dominated ocean layer would be gravitationally stable under ice VI layers or between overlying layers of ice VI–V or V–III.

## ACKNOWLEDGEMENTS

This work was partially supported by NASA Outer Planets Research through grants NNG06GF81G and NNX08AQ51G, by the National Science Foundation's IGERT program, grant number DGE-9870713, "IGERT: Astrobiology: Life in and beyond Earth's Solar System," by the Icy Worlds node of NASA's Astrobiology Institute (08-NAI5-0021) and the NASA and Caltech postdoctoral programs. Laboratory efforts benefited from substantial work by Evan Abramson, Nicholas Castle, Steven Domonkos, Kyle Straughn, and Hoku West-Foyle. Discussions with Evan Abramson are acknowledged and appreciated. Portions of this research were carried out at the Jet Propulsion Laboratory, California Institute of Technology, under a contract with the National Aeronautics and Space Administration. Copyright statement must be added until copyright is transferred to publisher.

## APPENDIX A. SUPPLEMENTARY DATA

Supplementary data associated with this article can be found, in the online version, at http://dx.doi.org/10.1016/j.gca.2013.01.040.

## REFERENCES

Abdulagatov I. M., Azizov N. D. and Zeinalova A. B. (2007) Viscosities, densities, apparent and partial molar volumes of concentrated aqueous $MgSO_4$ solutions at high temperatures and high pressures. *Phys. Chem. Liq.* **45**(2), 127–148.

Abramson E. H. and Brown J. M. (2004) Equation of state of water based on speeds of sound measured in the diamond-anvil cell. *Geochim. Cosmochim. Acta* **68**(8), 1827–1835.

Abramson E. H., Brown J. M. and Slutsky L. J. (1999) Applications of impulsive stimulated scattering in the earth and planetary sciences. *Annu. Rev. Phys. Chem.* **50**, 279–313.

Abramson E. H., Brown J. M., Slutsky L. J. and Wiryana S. (2001) Measuring speed of sound and thermal diffusivity in the diamond-anvil cell. *Int. J. Thermophys.* **22**, 405–414.

Anderson J. D., Lau E. L., Sjogren W. L., Schubert G. and Moore W. B. (1996) Gravitational constraints on the internal structure of Ganymede. *Nature* **384**(6609), 541–543.

Aster R. C., Borchers B. and Thurber C. H. (2012) *Parameter Estimation and Inverse Problems*. Academic Press.

Béghin C., Canu P., Karkoschka E., Sotin C., Bertucci C., Kurth W. S., Berthelier J. J., Grard R., Hamelin M., Schwingenschuh K. and Simões F. (2009) New insights on Titan's plasma-driven Schumann resonance inferred from Huygens and Cassini data. *Planet. Space Sci.* **57**(14–15), 1872–1888.

Béghin C., Sotin C. and Hamelin M. (2010) Titan's native ocean revealed beneath some 45 km of ice by a Schumann-like resonance. *C.R. Geosci.* **342**(6), 425–433.

Badarayani R., Patil K. R. and Kumar A. (2000) Experimental densities, speeds of sound, derived volumes and compressibilities of $H_2O$–KCl–$MgCl_2$–$CaCl_2$ and $H_2O$–KCl–$MgCl_2$–$CaCl_2$–NaCl systems at ionic strength 3 mol $kg^{-1}$ and at 298.15 K. *Fluid Phase Equilib.* **171**(1–2), 197–206.

Barr A. C., Pappalardo R. T. and Stevenson, D. J. (2001) Rise of deep melt into Ganymede's ocean and implications for astrobiology. In *Lunar and Planetary Institute Science Conference Abstracts*. pp. 1781.

Bethke C. (2008) *Geochemical and biogeochemical reaction modeling*. Cambridge Univ Press.

Bradley D. J. and Pitzer K. S. (1979) Thermodynamics of electrolytes. 12. Dielectric properties of water and Debye-Hueckel parameters to 350. degree. C and 1 kbar. *J. Phys. Chem.* **83**, 1599–1603.

Chen C., Emmet R. T. and Millero F. J. (1977) The apparent molal volumes of aqueous solutions of NaCl, KCl, $MgCl_2$, $Na_2SO_4$, and $MgSO_4$ from 0 to 1000 bars at 0, 25, and 50 °C. *J. Chem. Eng. Data* **22**(2), 201.

Choukroun M. and Grasset O. (2010) Thermodynamic data and modeling of the water and ammonia-water phase diagrams up to 2.2 GPa for planetary geophysics. *J. Chem. Phys.* **133**, 144502.

de Boor C. (2001) *A Practical Guide to Splines*. Springer, Berlin.

Denisov D. A. (2007) Calculation of the speed of sound in reciprocal systems from the known ion concentrations. *Acoust. Phys.* **53**(5), 589–593.

Denisov D. A., Abramov A. V. and Abramova E. P. (2003) A method for calculating the speed of sound in seawater. *Acoust. Phys.* **49**(4), 413–419.

Denisov D. A., Abramova E. P. and Abramov A. V. (2004) Calculation of the speed of sound in seawater from the known ion concentrations. *Acoust. Phys.* **50**, 609–613.

Dougherty M., Grasset O., Erd C., Titov D., Bunce E., Coustenis A., Blanc M., Coates A., Drossart P., Fletcher L. and others (2012) JUpiter ICy moons Explorer (JUICE): An ESA L-Class mission candidate to the Jupiter system. In *EGU General Assembly Conference Abstracts*. pp. 2260.

Fernandez D. P., Goodwin A. R. H., Lemmon E. W., Sengers J. M. H. L. and Williams R. C. (1997) A formulation for the static permittivity of water and steam at temperatures from 238 to 873 K at pressures up to 1200 MPa, including derivatives and Debye–Hückel coefficients. *J. Phys. Chem. Ref. Data* **26**, 1125.

Frantz J. D., Dubessy J. and Mysen B. O. (1994) Ion-pairing in aqueous $MgSO_4$ solutions along an isochore to 500 °C and 11 kbar using Raman spectroscopy in conjunction with the diamond-anvil cell. *Chem. Geol.* **116**(3–4), 181–188.

Gagnon R. E., Kiefte H., Clouter M. J. and Whalley E. (1990) Acoustic velocities and densities of polycrystalline ice Ih, II, III, V, and VI by Brillouin spectroscopy. *J. Chem. Phys.* **92**, 1909.

Grasset O., Mevel L., Mousis O. and Sotin C. (2001) The pressure dependence of the eutectic composition in the system $MgSO_4$–$H_2O$: implications for the deep liquid layer of icy satellites. *Lunar Planet. Inst. Sci. Conf. Abstr.* **32**, 1524.

Goodman J. C. and Lenferink E. (2012) Numerical simulations of marine hydrothermal plumes for Europa and other icy worlds. *Icarus* **221**(2), 970–983.

Hogenboom D. L., Kargel J. S., Ganasan J. P. and Lee L. (1995) Magnesium sulfate–water to 400 MPa using a novel piezometer: densities, phase equilibria, and planetological implications. *Icarus* **115**(2), 258–277.

Hu Y.-F. (2001) New predictive equations for the specific and apparent molar heat capacities of multicomponent aqueous solutions conforming to the linear isopiestic relation. *Bull. Chem. Soc. Jpn.* **74**, 47–52.

Hu Y.-F. and Fan S.-S. (2001) Estimating the speed of sound, compressibility, and thermal expansion for multicomponent solutions conforming to the linear isopiestic relation. *Fluid Phase Equilib.* **187**, 403–413.

Hussmann H., Sohl F. and Spohn T. (2006) Subsurface oceans and deep interiors of medium-sized outer planet satellites and large trans-neptunian objects. *Icarus* **185**, 258–273.

Iess L., Jacobson R. A., Ducci M., Stevenson D. J., Lunine J. I., Armstrong J. W., Asmar S. W., Racioppa P., Rappaport N. J. and Tortora P. (2012) The tides of Titan. *Science* **337**(6093), 457–459.

Johnson J. W., Oelkers E. H. and Helgeson H. C. (1992) SUPCRT92: a software package for calculating the standard molal thermodynamic properties of minerals, gases, aqueous species, and reactions from 1 to 5000 bar and 0 to 1000. *Comput. Geosci.* **18**(7), 899–947.

Khurana K. K., Kivelson M. G., Stevenson D. J., Schubert G., Russell C. T., Walker R. J. and Polanskey C. (1998) Induced magnetic fields as evidence for subsurface oceans in Europa and Callisto. *Nature* **395**(6704), 777–780.

Kivelson M. G., Khurana K. K. and Volwerk M. (2009) Europa's interaction with the jovian magnetosphere. In *Europa* (eds. R. T. Pappalardo, W. M. McKinnon, K. K. Khurana, with the assistance of René Dotson with 85 collaborating authors). *University of Arizona Press, Tucson. The University of Arizona space science series ISBN: 9780816528448, p. 545* **1**, 545.

Krumgalz B., Pogorelskii R., Sokolov A. and Pitzer K. (2000) Volumetric ion interaction parameters for single-solute aqueous electrolyte solutions at various temperatures. *J. Phys. Chem. Ref. Data* **29**(5), 1123–1140.

Krumgalz B. S., Starinsky A. and Pitzer K. S. (1999) Ion-interaction approach: pressure effect on the solubility of some minerals in submarine brines and seawater. *J. Solution Chem.* **28**(6), 667–692.

Lee S. W., Zanolin M., Thode A. M., Pappalardo R. T. and Makris N. C. (2003) Probing Europa's interior with natural sound sources. *Icarus* **165**(1), 144–167.

Lin C.-W. and Trusler J. P. M. (2012) The speed of sound and derived thermodynamic properties of pure water at temperatures between (253 and 473) K and at pressures up to 400 MPa. *J. Chem. Phys.* **136**, 094511.

Lo Surdo A., Alzola E. M. and Millero F. J. (1982) The (p, V, T) properties of concentrated aqueous-electrolytes. 4. Changes in the compressibilities of mixing the major sea salts at 25-degrees-C aqueous electrolytes I. Densities and apparent molar volumes of NaCl, $Na_2SO_4$, $MgCl_2$, and $MgSO_4$ solutions from 0.1 mol $kg^{-1}$ to saturation and from 273.15–323.15 K. *J. Chem. Thermodyn.* **14**(7), 649–662.

Madekufamba M. and Tremaine P. R. (2011) Ion association in dilute aqueous magnesium sulfate and nickel sulfate solutions under hydrothermal conditions by flow conductivity measurements. *J. Chem. Eng. Data* **56**(4), 889–898.

Marion G.M. and Grant S.A. (1994) *FREZCHEM: A chemical-thermodynamic model for aqueous solutions at subzero temperatures*. Technical report, DTIC Document.

Marion G. M., Kargel J. S., Catling D. C. and Jakubowski S. D. (2005) Effects of pressure on aqueous chemical equilibria at subzero temperatures with applications to Europa. *Geochim. Cosmochim. Acta* **69**(2), 259–274.

Marion G. M., Kargel J. S., Catling D. C. and Lunine J. I. (2012) Modeling ammonia–ammonium aqueous chemistries in the solar system's icy bodies. *Icarus* **220**, 932–946.

Melosh H. J., Ekholm A. G., Showman A. P. and Lorenz R. D. (2004) The temperature of Europa's subsurface water ocean. *Icarus* **168**(2), 498–502.

Millero F. J. (1983) *Influence of Pressure on Chemical Processes in the Sea*. Academic Press, London, pp. 1–87, Chapter 43.

Millero F. J. and Chen C. A. (1985) The speed of sound in mixtures of the major sea salts – a test of Young's rule for adiabatic PVT properties. *J. Solution Chem.* **14**(4), 301–310.

Millero F. J. and Knox J. (1973) Apparent molal volumes of aqueous $Na_2SO_4$, KCl, $K_2SO_4$, $MgCl_2$, and $MgSO_4$ solutions at 0 and 50 °C. *J. Chem. Eng. Data* **18**(4), 407–411.

Millero F. J. and Lampreia I. M. S. (1985) The PVT properties of concentrated aqueous-electrolytes. 4. Changes in the compressibilities of mixing the major sea salts at 25-degrees-C. *J. Solution Chem.* **14**(12), 853–864.

Millero F. J., Vinokurova F., Fernandez M. and Hershey J. P. (1987) PVT properties of concentrated electrolytes. VI. The speed of sound and apparent molal compressibilities of NaCl, $Na_2SO_4$, $MgCl_2$, and $MgSO_4$ solutions from 0 to 100 C. *J. Solution Chem.* **16**(4), 269–284.

Monnin C. (1989) An ion interaction model for the volumetric properties of natural waters: density of the solution and partial molal volumes of electrolytes to high concentrations at 25 °C. *Geochim. Cosmochim. Acta* **53**(6), 1177–1188.

Motin M. A. (2004) Temperature and concentration dependence of apparent molar volumes and viscosities of NaCl, $NH_4Cl$, $CuCl_2$, $CuSO_4$, and $MgSO_4$ in pure water and water + urea mixtures. *J. Chem. Eng. Data* **49**, 94–98.

Nakamura R. and Ohtani E. (2011) The high-pressure phase relation of the $MgSO_4$–$H_2O$ system and its implication for the internal structure of Ganymede. *Icarus* **211**(1), 648–654.

Phutela R. C. and Pitzer K. S. (1986a) Densities and apparent molar volumes of aqueous magnesium sulfate and sodium sulfate to 473 k and 100 bar. *J. Chem. Eng. Data* **31**(3), 320–327.

Phutela R. C. and Pitzer K. S. (1986b) Heat capacity and other thermodynamic properties of aqueous magnesium sulfate to 473 K. *J. Phys. Chem.* **90**, 895–901.

Pitzer K. S. (1973) Thermodynamics of electrolytes. I. Theoretical basis and general equation. *J. Phys. Chem.* **77**, 268–277.

Span R. (2000) *Multiparameter equations of state: an accurate source of thermodynamic property data*. Springer Verlag.

Sotin C. and Tobie G. (2004) Internal structure and dynamics of the large icy satellites. *C.R. Phys.* **5**(7), 769–780.

Vance S. and Brown J. M. (2005) Layering and double-diffusion style convection in Europa's ocean. *Icarus* **177**(2), 506–514.

Vance S. and Brown J. M. (2008). The simulator for icy world interiors, an apparatus for optical measurements in aqueous systems in the range −20 to 100 °C and 700 MPa. *Rev. Sci. Instrum.* **79**(1), 105105 1–5.

Vance S. and Brown J. M. (2010) Sound velocities and thermodynamic properties of water to 700 MPa and −20 to 100 °C. *J. Acoustic Soc. Am.* **127**(1), 174–180.

Vance, S. and Goodman, J. (2009). Oceanography of an ice-covered moon. In *Europa* (eds. R. T. Pappalardo, W. M. McKinnon, K. K. Khurana, with the assistance of René Dotson with 85 collaborating authors). *University of Arizona Press, Tucson. The University of Arizona space science series ISBN: 9780816528448*, pp. 459–482.

Vance S., Harnmeijer J., Kimura J., Hussmann H., deMartin B. and Brown J. M. (2007) Hydrothermal systems in small ocean planets. *Astrobiology* **7**(6), 987–1005.

Wagner W. and Pruss A. (2002) The IAPWS formulation 1995 for the thermodynamic properties of ordinary water substance for general and scientific use. *J. Phys. Chem. Ref. Data* **31**(2), 387–535.

Wiryana S., Slutsky L. J. and Brown J. M. (1998) The equation of state of water to 200 °C and 3.5 GPa: model potentials and the experimental pressure scale. *Earth Planet. Sci. Lett.* **163**, 123–130.

Wolery T. J. Laboratory, L. L. N. and of Energy, U. S. D. (1992), *EQ3/6: A software package for geochemical modeling of aqueous systems: package overview and installation guide (version 7.0)*, Lawrence Livermore National Laboratory.

*Associate editor:* Marc Norman